4-2-2006

Image Interpretation Using Appraisal Analysis

Partha S. Routh
Boise State University

Carlyle R. Miller
Boise State University

IMAGE INTERPRETATION USING APPRAISAL ANALYSIS

Partha S. Routh, Boise State University, Boise, ID
Carlyle R. Miller, Boise State University, Boise, ID

Abstract

In geophysical inversion, a significant effort is invested to obtain images of the Earth from finite data. The first step is to obtain an image i.e. solve the inverse problem. This step alone provides significant challenges that are not addressed in this paper. The next step is to interpret the image in terms of specific questions. For example, what can we say about the average value of a physical property within a certain region of the model? What scale information can we resolve from the data? These questions are problem dependent and may require that inversion be carried out several times to arrive at a satisfactory answer. Therefore the solution to an inverse problem is only a step towards answering these questions. Appraisal analysis of the solution takes the next step by providing a set of tools to judge and select from the possibly infinite suite of images that adequately fit our observations. We discuss the use of point spread functions and averaging kernels in the interpretation of images. We use a controlled source electromagnetic example to demonstrate the methodology.

Introduction

In this paper we focus on the image interpretation problem using appraisal analysis. Images obtained from inversion ultimately need to be interpreted in terms of physical property values, available structural information and/or questions that are connected with the image. Recognizing that a geophysical inverse problem is often non-unique and ill-posed due to limited data coverage and noise, we incorporate prior information into the inverse solution. As a result, the prior information is superposed on the inverse solution. Thus the scale of the model that can be resolved by inversion is affected by the sampling strategy of the data acquisition, associated data noise and the prior information that regularizes the ill-posed solution. Any prior information that we impose on our solution helps to supplement our unavoidably inadequate spatial and temporal data acquisition.

For a variety of applications it is difficult to establish a unified interpretation goal; however we can determine what regions of the image are influenced by prior information and what regions are constrained by the data. Although different ways to incorporate prior information are sometimes considered to be subjective (Friedel, 2003), it is an essential step in obtaining a stable solution that is physically meaningful. Often, we cannot neglect imposing prior information through the regularization procedure in the inverse problem. However, if we can develop some procedure to winnow out the regions that are not constrained by the data and the prior information then it would greatly simplify the interpretation and provide a robust way to connect the interpretation with the physical experiment that used to generate the data. Oldenburg and Li (1999) uses two different reference models in the nonlinear DC resistivity inversion to determine the regions of the inverted model that are honored by the data and then generate a filter function called depth of investigation (DOI) curves to interpret the inverted image. Alumbaugh and Newman (2000) uses 50% spread criteria from the point spread function to highlight the regions of the model that are better resolved. In seismic tomography, the impulse test and the checkerboard test are commonly applied. In these approaches, the raypaths of the real data are used on a synthetic impulse model or checkerboard model to generate the data. The inverted images are subsequently compared to the synthetic model to aid in understanding the model resolution (Shearer, 1999).

In this paper, we examine linearized appraisal analysis in detail. We use resolution measures such as the point spread functions and estimation measures such as the averaging kernels to examine the solution. One of the difficulties in using these measures is the excess information that needs to be summarized. Here we develop a spread criterion that summarizes these measures. There is no unique definition for the spread criteria, but having such a measure can greatly facilitate the interpretation process.

We begin the paper with discussion of the appraisal problem in both linear and nonlinear settings and make a clear distinction between the point spread functions that arise from the model construction process and the averaging kernels that provide the average value of the model parameters in a region. We then discuss the point spread function as a resolution measure for image interpretation.

Resolution Analysis in Inverse Problem

Insight into the resolution analysis problem can be gained by considering a linear inverse problem. This type of problem has been studied in great detail in previous literature, providing a path forward to examine the issues related to resolution and uncertainty (Backus and Gilbert, 1968; Backus and Gilbert, 1970; Oldenburg, 1983; Snieder, 1991; Parker, 1994; Alumbaugh and Newman, 2000; Alumbaugh, 2000). For a linear problem, $d^{obs} = Gm + \varepsilon$, the objective function ϕ to be minimized is given by

$$\phi = \left\| W_d \left(d^{obs} - Gm \right) \right\|^2 + \beta \left\| W_m \left(m - m_0 \right) \right\|^2 \qquad \text{.....(1)}$$

where $G \in R^{N \times M}$ is the forward modeling operator, $m \in R^M$ is the discretized model, $m_0 \in R^M$ is the reference model, $d^{obs} \in R^N$ is the data vector and $\varepsilon \in R^N$ is the vector of unknown data noise with the expectation $E(\varepsilon) = 0$ and the covariance matrix $C_d = \left(W_d^T W_d \right)^{-1}$. This linear system is usually ill-posed because of $M > N$ or ill-conditioned because G is not full column-ranked. W_d is the data weighting matrix that contains standard deviation of data errors. Denoting the Hessian by $H = \left(G^T W_d^T W_d G + \beta W_m^T W_m \right)$ the recovered model is given by

$$\hat{m} = H^{-1} G^T W_d^T W_d \, G \, m + H^{-1} G^T W_d^T W_d \;\; \varepsilon + H^{-1} W_m^T W_m \; m_0 \qquad \text{.....(2)}$$

The bias of the estimated model parameter can be represented by $E(\hat{m} - m) = H^{-1} W_m^T W_m (m_0 - m)$ since $E(\varepsilon) = 0$. Because the true model is unknown, the bias cannot be determined precisely, however, if we have knowledge about the norm of the true model then the bias can be bounded. In a more compact notation we can represent the estimated model in eq(2) by $\hat{m} = R \, m + \eta + \gamma$, where R is the resolution matrix given by

$$R = \left(G^T W_d^T W_d G + \beta W_m^T W_m \right)^{-1} G^T W_d^T W_d G \qquad \text{.....(3)}$$

R provides a mapping between the estimated model parameters, $\hat{m}$ and the true model parameters, m. For a nonlinear problem given by $d^{obs} = F(m) + \varepsilon$ the estimated solution for the model perturbation is given by

$$\delta\hat{m} = H^{-1} J^T W_d^T W_d \, J \, \delta m + H^{-1} J^T W_d^T W_d \left(Q(\delta m) - P(\delta\hat{m}) + \varepsilon \right) + H^{-1} W_m^T W_m \, \delta m_0 \ldots\ldots.(4)$$

where J is the sensitivity matrix, $Q(\delta m), P(\delta\hat{m})$ are the higher order terms typically neglected in the linearized analysis. Note when the higher order terms are not negligible it introduces bias into the solution of the estimated model perturbation. For our analysis we will neglect the higher order terms and carry out the interpretation using linearized analysis. We are particularly interested in the columns of the resolution matrix called the point spread functions (PSF). A PSF describes how a delta-like perturbation in the true model manifests itself in the inverted result. If a particular PSF is wide and/or has large side lobes, then the corresponding model is poorly resolved at that location and the resolution 'width' is broader than the cell dimension. The rows of the resolution matrix are the averaging or Backus-Gilbert (BG) kernels (Backus and Gilbert, 1970; Backus and Gilbert, 1968). These kernels show how the value of a specific model parameter is obtained by averaging the model in the entire domain. If the averaging kernel is a delta-like function at a certain location, then the contribution to the estimated value is obtained from that region and there is insignificant contribution from model parameters in other regions of the model. If we remove the effect of the reference model in eq(2) from the inversion then the average value of the model parameter can be represented by the following equation

$$\left\langle \hat{m} \right\rangle = \hat{m} - H^{-1} W_m^T W_m \, m_0 = R\, m + \eta \,. \qquad \ldots\ldots.(5)$$

The above equation shows that the average value of the model parameter is equal to the projection of the Backus-Gilbert (BG) averaging kernel (i.e row of R) onto the true model plus the noise contribution. Thus three quantities, the average value, $\left\langle \hat{m} \right\rangle_k$ the averaging kernel, $R(k,:)$ and the noise contribution, η_k should be interpreted together. PSF's are fundamentally different from BG kernels. The PSF is obtained from the model construction process and tells us about the resolving capacity of the inverse problem. The PSF provides insight about the inverse operator, and buried in the inverse operator are the effects of regularization due to a priori model constraints, model discretization, the kernels of the experiment and the effects of data noise (Routh et. al, 2005) . A BG kernel, on the other hand, is part of the averaging process and tells us how the true model parameters are averaged to provide us with the model estimate. Thus uncertainty in the model parameter estimates is associated with the averaging kernels and the associated noise.

Spread criteria for the Point Spread Function

Each PSF in a particular cell location tells us how a delta function is reconstructed during the model construction process. Thus the PSF contains significant information about the model. To compare the resolution capability of the data and prior information in different regions of the model, PSF's can be compared directly with each other. Although this is a valid procedure and has the ability to convey a significant amount of detail, the process can be tedious when we are faced with comparing thousands of cells in a large-scale experiment. We develop a spread criterion to summarize the information contained in the PSF to a single number. Note that definition of the spread criteria is non-unique, similar to the definition of attributes computed from time-frequency maps (Barnes, 1999; Sinha

et. al, 2005). For each cell, this number can be used as a diagnostic to compare the resolving capability of the inverse operator in different regions of the model. We propose the following definition of the spread

$$S(r_k) = \left[\frac{\int W(r, r_k)\left(p(r, r_k) - \delta(r - r_k)\right)^2 dr}{\alpha + \int p^2(r, r_k) dr} \right]^{1/2} \qquad \text{.....(6)}$$

where $W(r, r_k)$ is a distance weighting matrix that increases the spread value when there are side lobes away from the region of interest. $p(r, r_k)$ is the point spread function for the cell whose center is at r_k and α is a small threshold parameter chosen so that the denominator in the spread equation is not equal to zero when the energy of the point spread function is zero. Zero PSF can occur in regions of insufficient data coverage. If the PSF peak is shifted from the region of interest, the chosen spread criteria will generate large spread values. In the next section we demonstrate the use of the PSF and spread criteria to interpret inverted models obtained from a frequency domain controlled source EM experiment.

Example from Controlled Source Electromagnetic (CSEM) data

We consider a synthetic controlled source audio-frequency magnetotelluric (CSAMT) experiment to demonstrate the methodology. In CSAMT, harmonic current at different frequencies is transmitted into the ground and multi-component electric and magnetic field data are measured at each frequency. Figure 1 shows the amplitude and phase data of electric and magnetic field components as a function of frequency. These data are generated using a transmitter located 2 km from the receiver and a frequency bandwidth of 0.5-8192 Hz sampled logarithmically. The amplitude data are contaminated with noise amounting to 5% of the standard deviation of the datum value and the phases are contaminated with 3 degree standard deviation. The Earth model is discretized using a 1D, 80 layer model with layer thickness increasing logarithmically. The electrical conductivity of the synthetic model varies with depth, as shown in Figure 3. Data are inverted using a nonlinear Gauss-Newton approach outlined in Routh and Oldenburg, 1999. A constant electrical resistivity value of 100 Ωm was used as the reference model for the inversions. Various combinations of the fields are inverted to examine the contribution of multi-component data, shown in Figure 3. Figure 2 shows the resolution matrices obtained from the final model of the inversion. Regardless of their differences we note that the depths below the 50^{th} layer are not resolved by the available data.

The PSF's obtained from different component inversions are shown in Figure 3. It indicates that the conductive layer at the depth of 500m is better resolved compared to the resistive layer at the depth of 200m. Regions with larger conductive anomalies will focus the currents in the subsurface. Since CSAMT has both galvanic as well as inductive currents the synthetic example indicates that the conductor is better resolved than the resistive layer due to current gathering. The physical insight is that the diffusive currents are slower in a conductive region and faster in resistive regions. Therefore resolving capability is better for a conductive target. Comparing the PSFs with different components suggests that the electric field has better resolving capability compared to the magnetic field.

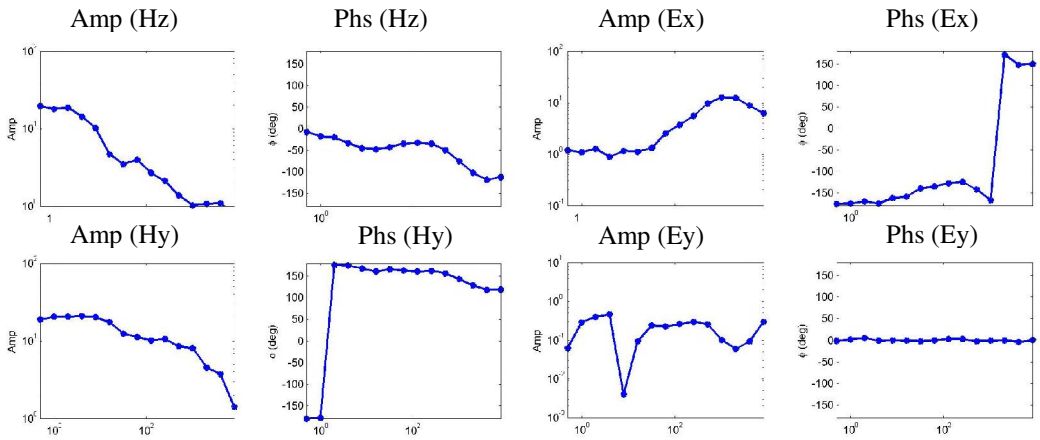

Figure 1: The $\log_{10}$(amplitude) (μV/m for E and μH/m for H) and phase in degrees for multi-component CSAMT data as a function of $\log_{10}$(frequency) in the range of 0.5-8192 Hz.

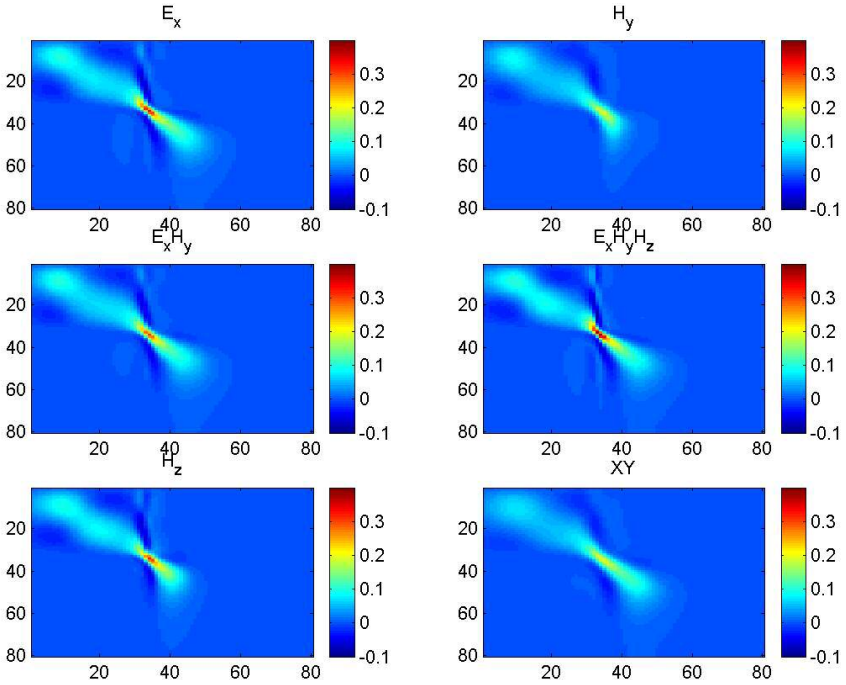

Figure 2: The resolution matrix R, obtained from the final iteration of the inversion for different components of the fields. The Earth model has 80 layers and therefore the size of R is 80 x 80. The plot clearly indicates that the data are unable to resolve the depths beyond the 50th layer. It also shows that the conductive region is better resolved compared to the rest of the model. The bottom right panel gives the resolution matrix for the inversion of the apparent resistivity data, ρ_{xy}.

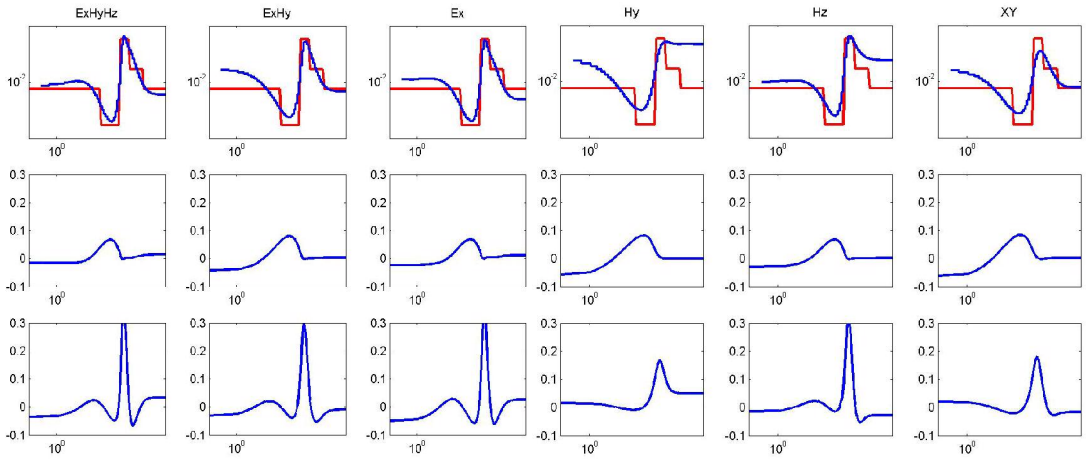

Figure 3: Top panel: Models obtained by inverting different components of the field individually or in combination. For the top panel, the vertical axis is the resistivity (Ωm), and the horizontal axis is the depth (m). The blocky red line shows the synthetic model used in generating the data. The far right plot is for the XY component of the apparent resistivity and phase, ρ_{xy}. The middle panel shows the PSF's for the resistive layer and the bottom panel shows the the PSF's for the conductive layer.

Next we compare the averaging functions- the rows of the resolution matrix. Figure 4 shows that the averaging functions for the conductive layer is closer to a delta-like function when compared to the resistive layer. Thus the uncertainty in the value of the conductive layer is smaller compared to the resistive region.

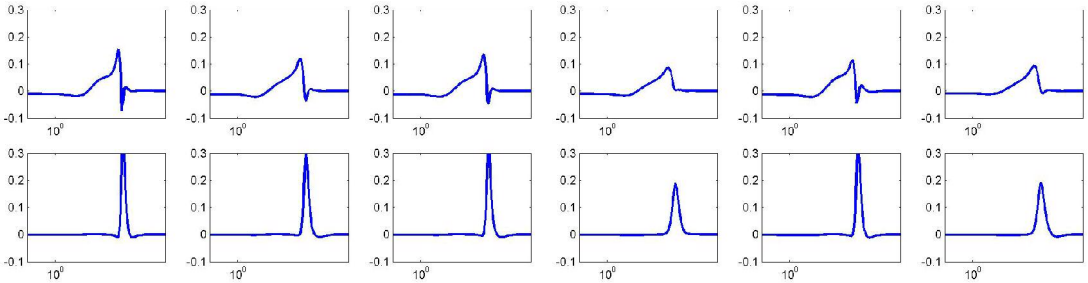

Figure 4: Averaging kernels obtained by inverting different components of the field individually or in combination (order is same as in Figure 3). The top panel shows the averaging kernels for the resistive layer. The bottom panel shows the averaging kernels for the conductive layer.

Having examined the PSF's and the averaging kernels our next step is to examine the spread function in the entire model domain. Equation (6) is used to compute the spread for the multi-component inversions. The spread diagram in Figure 5 clearly indicates that the magnetic field has poor resolution in the deeper part of the model compared to the electric field. In addition, the plot shows that the inversion of apparent resistivity and phase data have poor resolution compared to the direct inversion with the fields. Because apparent resistivity is a nonlinear transform of the fields it decreases the signal to noise ratio resulting in poor resolving capability (Routh and Oldenburg, 2000). The spread criteria plot summarizes the resolving capability of the experiment in the entire model domain. Regions that are poorly resolved will have larger spread value. Thus from an interpretation point of view a map of the spread criteria is a useful tool to place confidence on the inverted model.

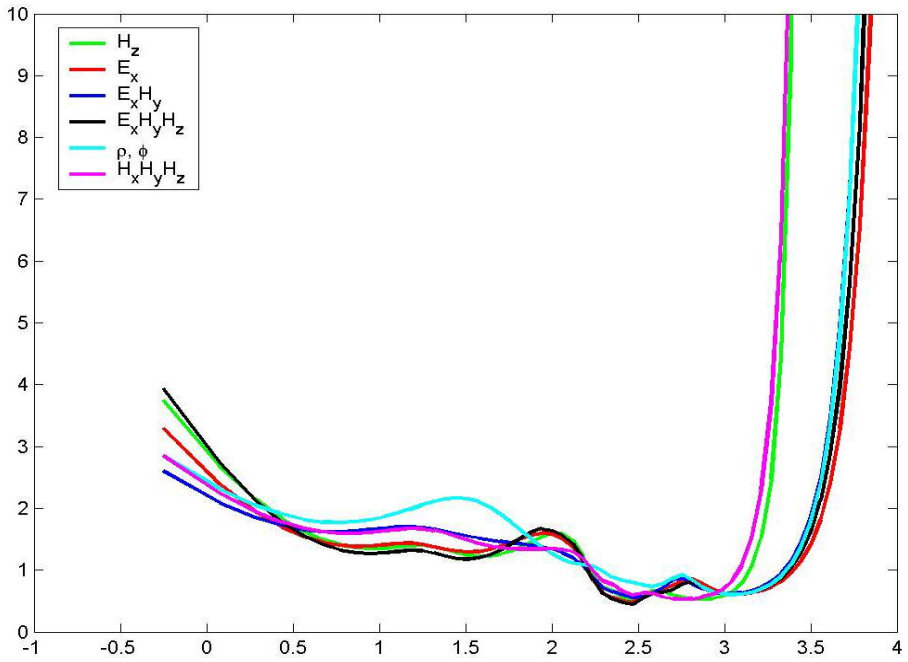

Figure 5: Spread computed from the PSFs obtained at the final iteration of the inversion. The x-axis is the depth plotted in the log scale i.e. $\log_{10}$(z (m)).

To illustrate the utility of the spread measures we consider two data sets i.e. ExHyHz and HxHyHz. The spread curves for these two cases are shown in Figure 6. To interpret these spread curves we chose a level set i.e. an iso-spread value for the entire depth region shown by the horizontal line in the top panel in Figure 6. If the spread values lie above this line then the regions are poorly resolved. The end points of the intersection between the level set and the spread curve roughly defines the domain of the model that is resolved by the experiment. At larger depths this intersection can be interpreted as the depth of investigation of the particular data set. Figure 6 shows that the depth of investigation with ExHyHz is greater than with HxHyHz. As discussed earlier this is an expected result since the Ex component has better depth information compared to the magnetic field. Using this interpretation our next step is to winnow the regions of the model that are below this resolution limit. In Figure 7 we demonstrate how this information can be used to truncate the regions of the model that are within the resolving capacity. The bottom panels in Figure 7 shows regions of the model constrained by the data. Inversion with the electric field data shows a larger model region that can be resolved from the available data compared to the magnetic field. To further investigate the uncertainty of the values in the truncated region, the averaging function can be considered. Employing a similar approach to the one used for the PSF, one can generate a spread map with the averaging function within the resolved zones to compare the uncertainty in the average values of the model parameters (not shown).

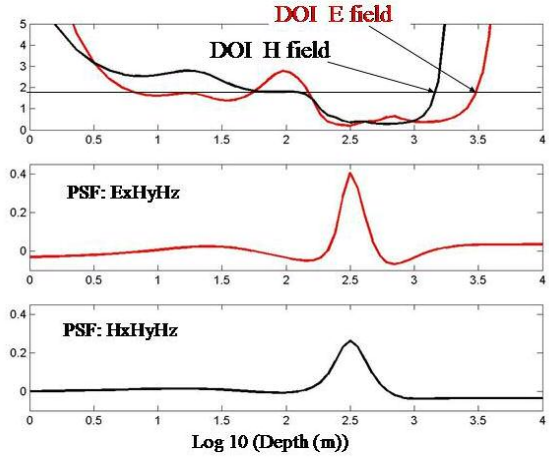

Figure 6: The top panel shows the spread function for the ExHyHz and HxHyHz field inversion. The level set indicated by the horizontal line indicates an iso-spread value chosen to examine the depth of investigation (DOI) of the fields. The middle and bottom panels are the PSFs of the conductive layer.

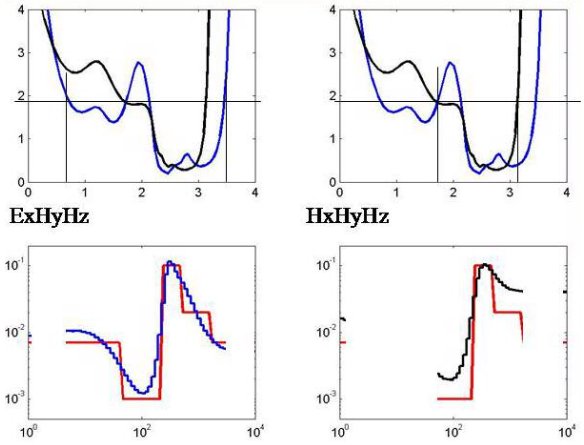

Figure 7: The top left and right panel shows the spread curves for the ExHyHz (blue) and HxHyHz (black). The level set for the spread value is shown by the black horizontal line. The vertical line on the spread plot shows the depth interval resolved by the data. The bottom left and right panels show the region of the model that is resolved by the available data.

Discussion and Conclusions

Geophysical data are inherently noisy and inadequately sampled. The practical limitations in most geophysical data acquisition are logistical considerations in terms of spatial and/or temporal sampling. However, the model that we seek to obtain from the data via an inversion paradigm is heterogeneous at multiple scales. Therefore with a particular survey we are limited in terms of illuminating the various scales of the heterogeneous structure, thus hindering our capability to describe and understand the physical processes. The spatial sampling of data plays a major role in determining what structures can be resolved and finally interpreted. This is the central issue in the resolution analysis. In addition, the superposition of the noise on the signal introduces further non-uniqueness in the solution. To forward model the data we typically discretize the model finely enough so that there are no errors introduced due to coarse discretization. Thus we have many more degrees of freedom with the model and insufficient data to recover them. Faced with this non-uniqueness our strategy is to impose constraints in the model subject to fitting the data within some tolerance level. Thus the final model

obtained from inversion is influenced by (a) the physics of the experiment i.e. the data, (b) the a priori information that was incorporated to overcome the ill-posed nature of the solution and (c) the noise component that cannot be explained by the forward model. In this paper we show a detailed analysis on how to use the point spread functions and the averaging kernels to help interpret an image. The procedure presented here is restricted to the linearized analysis but insight gained through this method can be useful for making decisions with practical implications.

Acknowledgements

We thank Environmental Protection Agency Grant EPA-X-96004601. Part of this work is also funded by NSF-EPSCOR grant and Boise State Faculty Research grant to PSR. We thank Inland Northwest Research Alliance (INRA) fellowship to Carlyle Miller.

References

Alumbaugh, D., 2000, Linearized and nonlinear parameter variance estimation for two-dimensional electromagnetic induction problem, Inverse Problems, 16, 1323-41.

Alumbaugh, D., and Newman, G., 2000, Image appraisal in 2D and 3D electromagnetic inversion, Geophysics, 65, 1455-67.

Backus, G., and Gilbert, F., 1968, The resolving power of gross earth data, Geophy. J. Royal Astr. Soc., 16, 169-205.

Backus, G., and Gilbert, F., 1970, Uniqueness in the inversion of gross earth data, Phil. Trans. Roy. Soc. Series A Mathematical and Physical Sciences, 266, 123-192.

Barnes, A., 1993, Instantaneous spectral bandwidth and dominant frequency with seismic reflection data, Geophysics, 58, 419-428.

Friedel, S., 2003, Resolution, stability and efficiency of resistivity tomography estimated from a generalized inverse approach, Geophy. J. Inter., 153, 305-316.

Oldenburg, D., 1983, Funnel functions in linear and nonlinear appraisal, J. Geophy. Res., B 9 7387-98.

Oldenburg, D., and Li, Y., 1999, Estimating the depth of investigation in dc resistivity and IP surveys, Geophysics, 64, 403-416.

Parker, R., 1994, Geophysical Inverse Theory, Princeton University Press.

Routh, P., and Oldenburg, D., 2000, Advantages of field component inversion of CSAMT data, SEG expanded abstracts, Vol. I, 261-264.

Routh, P., S., and Oldenburg, D., W., 1999, Inversion of controlled source audio-frequency magnetotelluric data for a horizontally layered Earth, Geophysics, 64, no. 6, 1689-97.

Routh, P., S., Oldenborger, G. A., and Oldenburg, D. W., 2005, Optimal survey design using resolution measure of point spread function, SEG Expanded Abstracts, 1033-1036.

Shearer, P., 1999, Introduction to Seismology, Cambridge University Press.

Sinha, S., Routh, P., Anno, P., and Castagna, J., 2005, Scale attributes from continuous wavelet transform, SEG expanded abstracts, 779-781.

Snieder, R., 1990, A perturbative analysis of nonlinear inversion, Geophy. J. Inter., 101, 545-556.